Scattering Dynamics with Gaussian Potential in the Presence of a Bichromatic Laser Field

Santosh Kumar Das, Saddam Husain Dhobi*

Department of Physics, Patan Multiple Campus, Tribhuvan University, Patandhoka, Lalitpur-44700, Nepal

Research Article

ISSN: 3059-9504 (online)
DOI: https://doi.org/ 10.3126/ajs.v2i1.87752

Article History

Received: August 15, 2025; Revised: November 07, 2025; Accepted: November 10, 2025; Published: December 25, 2025

Keywords

Differential cross section, Gaussian potential, laser field, Scattering dynamics, Volkov wave equation.

***Corresponding author**

Email: saddam@ran.edu.np
dassantosh29@gmail.com (SH Dhobi)

ABSTRACT

Scattering dynamics play a crucial role in understanding the fundamental interactions between particles and external fields. When a particle interacts with a target potential under the influence of an external laser field, its motion and energy distribution can be significantly modified. The aim of this work is to study the scattering dynamics of electron-gaussian potential in presence of bichromatic linearly polarized laser fields. To fulfill the objective, we obtained S-matrix use Volkov wave equation and Gaussian potential with the help of Kroll-Watson approximation. Using relation of S-matrix and T-matrix, the obtained T-matrix which is directly related to differential cross section (DCS). The obtained DCS used to study the scattering dynamics of electron behavior with gaussian potential in laser field. The developed DCS equation was computed, the computed result shows DCS increases with increase of incidence energy of electron and becomes maximum and finally decreases. The DCS with photon energy is highly fluctuations and decrease with increase of scattering angle. The DCS of Bessel first order found greater than Bessel second order. These findings aid in laser-assisted collision studies, plasma diagnostics, nanomaterial design, and quantum device optimization by revealing electron behavior, multiphoton effects, and resonance control under bichromatic laser fields.

1. INTRODUCTION

This study investigates DCS in the presence of a linearly polarized laser field, employing Bessel functions of varying orders, with oxygen molecules modeled under the Lennard-Jones potential. The analysis demonstrates that electron energy can be absorbed or emitted during interactions, producing pronounced resonance peaks in the DCS, which indicate potential formation of new particle structures, while minima correspond to strong electron–target coupling and smaller composite formation. The Bessel zero-order exhibits higher DCS values compared to higher orders, and at zero-radian scattering angle, the DCS reaches its minimum, emphasizing enhanced particle interactions at this orientation [1]. Analytical studies using the coupled-channel Lippmann–Schwinger equation for a one-dimensional δ-function potential further show that electrons can absorb or emit energy in integer multiples of the laser frequency, resulting in elastic, inelastic, and superelastic scattering amplitudes with observed stimulated recombination resonances [2]. Accurate modeling of laser-assisted multiphoton transitions also requires consideration of realistic laser field properties, including focusing, pulse structure, multimode behavior, and statistical fluctuations, which significantly affect scattering cross sections in fast electron–atom collisions [3]. Previous studies have explored electron-laser interactions using attractive δ-function potentials, primarily through numerical solutions of the time-dependent Schrödinger equation, focusing on photoionization rates in strong-field regimes (10^9–10^{14} W/cm²), while ultra strong-field domains (≥10^{16} W/cm²) remain less examined. Laser-modified scattering rates for this potential are not well-studied, though related phenomena have been analyzed in other systems, showing stabilization of bound states under high-intensity fields [2]. The Kroll–Watson approximation is widely employed, treating electron-laser interaction nonperturbatively but neglecting direct laser-atom coupling, predicting that the field-free scattering cross section is modified mainly by electron-laser interactions [4]. In strong fields, electrons can undergo scattering, leading to above-threshold ionization, harmonic generation, and further excitations [5], while intense lasers enhance charge exchange in ion-atom collisions under resonant conditions [6]. Quantum-orbit theory effectively describes multistep processes [7] by Milošević et al. Realistic laser models incorporating multimode behavior and pulse shaping are essential for accurate light-matter interaction simulations [8]. Correlated double ionization highlights strong electron correlation in multiphoton ionization [9], and ponderomotive effects dominate electron-photon scattering in high-intensity fields [10]. Beyond fundamental physics, laser microtechnology enables precise fabrication of micrometer-scale structures for optics and electronics applications [11].

The scattering dynamics of particles interacting with a Gaussian potential in the presence of a bichromatic laser field is a complex

phenomenon studied within atomic physics and laser-matter interaction, integrating concepts from quantum mechanics and electromagnetism [12-15]. A Gaussian potential is often employed in theoretical models due to its analytical tractability and its ability to represent localized interactions, such as those occurring in quantum dots or screened atomic potentials. The presence of a bichromatic laser field, which consists of two laser components with different frequencies (e.g., ω and 2ω or ω and 3ω) and a controllable relative phase, introduces a powerful tool for coherent control of scattering processes [16-17]. The theoretical framework for analyzing such interactions typically involves solving the time-dependent Schrödinger equation or employing approximations like the Born approximation, particularly the first and second Born approximations. The Volkov wave functions are often used to describe the states of electrons in the presence of a strong laser field [18]. These approaches allow for the calculation of DCS and total differential cross sections, which are crucial for understanding the probability and angular distribution of scattered particles [19].

Despite extensive studies on laser-assisted scattering using monochromatic fields and simple potentials, the effects of Gaussian potentials under bichromatic laser fields remain underexplored, particularly regarding phase-dependent, multiphoton interactions, and nonlinear frequency-dependent effects. Most prior work has focused on δ-function or Lennard-Jones potentials, often neglecting realistic laser properties and coherent control over electron dynamics. Investigating electron scattering in a bichromatic field composed of two frequencies (e.g., ω and 2ω or ω and 3ω) with a controllable relative phase provides enhanced flexibility, enabling precise manipulation of energy and momentum transfer, resonances, and multiphoton processes. Understanding these dynamics is crucial for laser-assisted collision studies, plasma diagnostics, nanomaterial design, and quantum device optimization, as it reveals detailed electron behavior under realistic experimental conditions and allows coherent control that monochromatic fields cannot achieve.

2. MATERIALS AND METHODS

The time dependent Schrödinger equation can be used to describe the conduction-band electrons dynamics in the (x,y) plane [15, 20] as:

$$\left[\frac{1}{2\mathrm{m}'}\left(\mathbf{p}-\frac{\mathrm{e}}{\mathrm{c}}\mathbf{A}(\mathrm{t})\right)^2+\mathrm{V}(\mathrm{r})\right]X(\mathrm{x},\mathrm{y},\mathrm{t})=\ \mathrm{i}\hbar\frac{\partial X(\mathrm{x},\mathrm{y},\mathrm{t})}{\partial \mathrm{t}} \quad (1)$$

represents the time-dependent Schrödinger equation for an electron in the presence of an external electromagnetic field, where m' is the electron mass, **p** is the momentum operator, e is the electron charge, c is the speed of light, **A**(t) is the time-dependent vector potential, and V(r) is the potential energy. The term $\left(\mathbf{p}-\frac{\mathrm{e}}{\mathrm{c}}\mathbf{A}(\mathrm{t})\right)^2$ accounts for the coupling between the charged particle and the electromagnetic field through the minimal coupling scheme, while the right-hand side describes the time evolution of the wave function $X(\mathrm{x},\mathrm{y},\mathrm{t})$. The corresponding solution of equation (1) is presented in equation (2) [21-24].

$$X(r,t)=\frac{1}{(2\pi)^{\frac{3}{2}}}\exp\left\{i\frac{\boldsymbol{p}}{\hbar}.\left(\boldsymbol{r}+\frac{\mathrm{e}}{\mathrm{m}'}\int\mathbf{A}(\,t)dt\right)-i\frac{E}{\hbar}t-\right.$$
$$\left.i\frac{\mathrm{e}^2}{2\mathrm{m}'\hbar}\int\mathbf{A}^2(t)\,dt\right\} \quad (2)$$

which is known as the Volkov wave function, describing a free electron dressed by the electromagnetic field; here $\boldsymbol{r}$ is the position vector, E is the electron energy, and the exponential terms represent, respectively, the plane-wave contribution, the phase modulation due to the vector potential, and the additional phase shift arising from the field intensity through the $\int\mathbf{A}^2(t)dt$ term. The vector potential for bichromatic linear polarized laser [25].

$$\mathbf{A}(t)=\epsilon_1\left(\frac{\varepsilon_1}{\omega}\right)\cos(\omega t)+\epsilon_m\left(\frac{\varepsilon_m}{m\omega}\right)\cos(m\omega t+\phi) \quad (3)$$

where ϵ_1 and ϵ_m denote the independent polarization vectors. For simplicity, both fields are assumed to have the same linear polarization. Here, ε_1 and ε_m represent the corresponding electric field strengths, while ϕ indicates the relative phase. In practical applications, the parameter m typically takes the values 2 or 3, corresponding to the second and third harmonics. Experimentally, the achievable ratio $\varepsilon_m/\varepsilon_1$ is usually around 10% in nonlinear media, and this ratio is even smaller for the third harmonic. Now putting value of **A**(t) form equation (3) in equation (2) and solving as:

$$X(r,t)=\frac{1}{(2\pi)^{\frac{3}{2}}}\exp\left\{i\frac{p}{\hbar}.\left(r+\frac{e}{m'}\int\boldsymbol{\epsilon_1}\ \left(\frac{\epsilon_1}{\omega}\right)\boldsymbol{cos}\omega t+\right.\right.$$
$$\left.\epsilon_m\left(\frac{\epsilon_m}{m\omega}\right)cos(m\omega t+\phi)\,dt\right)-i\frac{E}{\hbar}t-$$
$$\left.i\frac{e^2}{2m'\hbar}\int\left(\boldsymbol{\epsilon_1}\left(\frac{\epsilon_1}{\omega}\right)\boldsymbol{cos}\omega t+\ \epsilon_m\left(\frac{\varepsilon_m}{m\omega}\right)cos(m\omega t+\phi)\right)^{\mathbf{2}}\right\} \quad (4)$$

Equation (4) represents the wavefunction of a charged particle in an oscillating electromagnetic field, known as the Volkov-type solution. Physically, it describes how the particle's phase and motion are modified by the presence of combined laser fields the fundamental frequency ω and its harmonic $m\omega$ (usually $m=2$ or 3). On integration Equation (4) and solving with omitting last term of equation (4) because it is very small in magnitude and it doesn't play the vital role. When system is unperturbed due to laser field then we apply Kroll-Watson Approximation for perturbation. S-matrix is used to get the system information and it is also used when times tends to infinity

$$X(r,t)=\frac{1}{(2\pi)^{\frac{3}{2}}}\exp\left\{iprcos\theta+ip\left[\epsilon_1\left(\frac{\varepsilon_1}{\omega^2}\right)\sin(\omega t)-\right.\right.$$
$$\left.\left.\epsilon_m\left(\frac{\varepsilon_m}{m\omega^2}\right)\sin(m\omega t+\phi)\right]-iEt\right\} \quad (5)$$

Physically, this equation emphasizes how the particle's position and phase vary with time due to the external electric fields, while neglecting the overall phase factor that has no observable effect. The term $prcos\theta$ accounts for the propagation of the wave in space, and the sine-dependent terms represent the field-driven

displacement of the electron caused by the oscillating components of the electric field. Thus, equation (5) captures the essential dynamic behavior of the system in a simplified form, focusing only on the physically meaningful, time-dependent motion. Now using Kroll-Watson Approximation S-matrix [26-28] is defined as

$$S_{fi}^{E} = \delta_{fi} - \frac{i}{\hbar}\int_{-\infty}^{\infty} \langle X_f(r,t)|V(r)|X_i(r,t)\rangle \, dt \qquad (6)$$

Where Equation (6) represents, the S-matrix with transition amplitude [second term of Equation (6)] between an initial quantum state $X_i(r,t)$ and a final state $X_f(r,t)$ under the influence of an interaction potential $V(r)$. Physically, this equation comes from time-dependent perturbation theory and describes how an external field or potential induces a transition between two quantum states. The first term, δ_{fi}, corresponds to the case where no interaction occurs (the system remains in the same state), while the second term gives the probability amplitude for transition due to the perturbing potential. The integral over time accounts for the accumulated effect of the interaction throughout the field's duration. The second term of equation (6) for transition matrix or T-matrix is obtained with the help of Equation (7),

$$T_{fi} = \int_{-\infty}^{\infty} \left\langle X_f(r,t)\middle|V(r)|X_i(r,t)\right\rangle dt \qquad (7)$$

Physically, it quantifies how strongly and effectively the interaction couples the two states over time. A larger value of T_{fi} indicates a higher probability of transition, meaning the potential $V(r)$ strongly influences the particle's motion. In laser–matter or scattering processes, this term is crucial for determining transition probabilities, cross-sections, and emission or absorption rates, reflecting how external fields or potentials drive the exchange of energy between the system and its environment. After putting the value of wave function equation (5) on equation (7) and solving we get,

$$T_{fi} = \int d^3r \int_{-\infty}^{\infty} \left(\frac{1}{(2\pi)^{\frac{3}{2}}} \exp\left\{ -ip_f r cos\theta - ip_f \left(\epsilon_1 \left(\frac{\varepsilon_1}{\omega^2}\right) \sin(\omega t) - \epsilon_m \left(\frac{\varepsilon_m}{m\omega^2}\right) \sin(m\omega t + \phi) \right) + iE_f t \right\} V(r) \; \frac{1}{(2\pi)^{\frac{3}{2}}} \exp\left\{ ip_i r cos\theta + ip_i \left(\epsilon_1 \left(\frac{\varepsilon_1}{\omega^2}\right) \sin(\omega t) - \epsilon_m \left(\frac{\varepsilon_m}{m\omega^2}\right) \sin(m\omega t + \phi) \right) - iE_i t \right\} \right) dt \qquad (8)$$

After performing the time integral with the Jacobi–Anger expansion, the oscillatory factors turn into sums of Bessel functions (J_n) and the time integral produces a Kronecker/Dirac delta enforcing discrete energy balance in Equation (8). Physically that result has two immediate meanings: (a) the Bessel functions give the amplitude for absorbing/emitting n photons from a given harmonic component, so they set the relative strength of each multiphoton channel; and (b) the Kronecker/energy delta implements energy conservation. The final equation (8) after solving we get equation (9) as,

$$T_{fi} = \frac{1}{(2\pi)^3} \int \{ \exp(ikr) \times J_n(dn_1) \times J_n(dn_2) \exp(in\phi) \} V(r) d^3r \qquad (9)$$

Where $dn_1 = k\epsilon_1 \left(\frac{\varepsilon_1}{\omega^2}\right)$ *and* $dn_2 = -\epsilon_m \left(\frac{\varepsilon_m}{m\omega^2}\right)$ and $d^3r = r^2 sin\theta \; d\theta \; d\phi \; dr$ represent the volume for spherical coordinate system and $k = k_f - k_i$. On putting the value of V(r) which is known as Gaussian potential [29] defined in Equation (10) as,

$$V(r) = V_0 \exp\left\{ -\left(\frac{r}{R}\right)^2 \right\} \qquad (10)$$

Physically, V_0 defines the depth or strength of the potential well, while R specifies its spatial extent or characteristic range, the region within which the interaction is significant. The exponential decay ensures that the potential rapidly approaches zero as r increases, meaning the particle experiences a strong interaction only near the center and is essentially free beyond that region. On substituting the value form equation (10) to equation (9) and solving we get the T-matrix as

$$T_{fi} = -\frac{V_0 J_n(dn_1) J_n(dn_2) \exp(in\phi)}{4\pi^2 ik} \left\{ \begin{array}{c} \sqrt{\pi} \; (ikcos\theta) \exp\left(-\frac{(kcos\theta)^2 R^2}{4} \right) \frac{R^3 \, erf\left(\frac{2r}{R^2} - ikcos\theta\right)}{8\sqrt{ikcos\theta}} - \\ \frac{R^2 \exp\left(r \left\{ ikcos\theta - \frac{r}{R^2} \right\} \right)}{2} \end{array} \right\} \qquad (11)$$

Equation (11) is final equation of transition matrix which is directly related to DCS and this transition matrix is used to study the scattering dynamics of electron with gaussian potential in laser field. Since we have relation of DCS and transition matrix [30-32] we have,

$$\frac{d\sigma}{d\Omega} = \frac{k_f}{k_i} \left| T_{fi} \right|^2 \qquad (12)$$

Equation (12) shows relationship between the transition matrix element and the DCS, which quantifies the probability of an electron being scattered into a specific solid angle $d\Omega$. Physically, this equation shows that the DCS depends on the magnitude squared of the transition amplitude, representing the strength of interaction between the incoming and outgoing states. The transition matrix T_{fi}, derived from equation (11), encapsulates all the effects of the laser field, Gaussian potential, and multiphoton interactions. Now substituting value from equation (11) to equation (12) we get final equation (13) to study the scattering dynamics of electron and gaussian potential as

$$\frac{d\sigma}{d\Omega} = \frac{k_f}{k_i} \left| -\frac{V_0 J_n(dn_1) J_n(dn_2) \exp(in\phi)}{4\pi^2 ik} \left\{ \sqrt{\pi} \; (ikcos\theta) \exp\left(-\frac{(kcos\theta)^2 R^2}{4} \right) \frac{R^3 \, erf\left(\frac{2r}{R^2} - ikcos\theta\right)}{8\sqrt{ikcos\theta}} - \frac{R^2 \exp\left(r \left\{ ikcos\theta - \frac{r}{R^2} \right\} \right)}{2} \right\} \right|^2 \qquad (13)$$

Equation (13) gives the DCS for an electron scattering from a Gaussian potential in the presence of a two-color laser field. Physically, it combines the effects of the laser-driven multiphoton processes (through Bessel functions and the relative phase ϕ), the spatial characteristics of the Gaussian potential (strength V_0 and range R, including error-function and exponential terms from spatial integration), and the kinematic/angular dependence of the scattering ($k_i, k_f, \cos\theta$). The modulus squared represents the probability of the electron being scattered into a specific angle, showing how the laser field, potential shape, and scattering geometry together control the angular distribution and intensity of the scattered electrons.

3. RESULTS AND DISCUSSION

Computational detail: Change in momentum (1-4) eV, strength of the potential well 2.7× 10^{-10}mV, Bessel order (1-5), harmonic order (2-3), $r = 1$ Å, $R = 0.6 - 0.8$ Å, scattering angle (0-120°), polarization vectors ($\epsilon_1 = \epsilon_m = 1$), electric field strength ($\varepsilon_1 = 1\ a.u.$ and $\varepsilon_m = 2\ a.u.$), phase angle (5.7° and 57°). Figure 1 illustrates the variation of the DCS with photon incidence energy in the presence of a laser field for the Bessel first-order. The analysis revealed that Figure 1(a) corresponds to the second-order harmonic ($m = 2$), while Figure 1(b) represents the third-order harmonic ($m = 3$). Also, the harmonic order of the laser field increases, the DCS decreases for the Bessel first-order. This reduction is attributed to the decrease in field amplitude at higher harmonic orders. Furthermore, shift in maxima peak towards lower photon incidence energy is observed with increasing harmonic order. On the other hand, the maxima peak for the $m = 2$ appears at approximately 1.7 eV and the $m = 3$ around 1.9 eV. The peak was due to superposition of amplitude of projected, target and laser where project is nearer to target.

The demonstrate shows dependency of the DCS on the harmonic order of the applied laser field. The increasing in harmonic order shows the DCS decreases due to the reduction in field amplitude as it is directly related to DCS. The maxima peak for $m = 2$ and $m = 3$, suggests lower-order harmonics the probability of scattering is higher means weaker interaction while higher-order harmonic the probability of scattering is lower and interaction is higher. This means scattering dynamic of electron with gaussian potential is higher for lower order harmonic. In lower energy region below 10 eV [33] show that DCS initially increase with increasing in scattering electron energy and become maximum and then decrease for electron-atom in two polarized colors. Also Figure 1 and Figure 2 has similar nature obtained by Bartschat et al. [34] where they study quantum-mechanical calculations of cross sections for electron collisions with atoms and molecules.

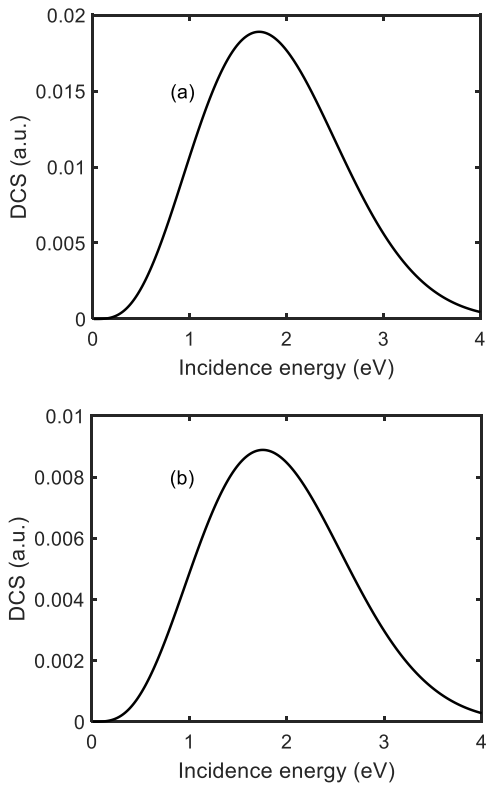

Fig. 1: DCS with incidence energy of electron (a) $m = 2$ and (b) $m = 3$ for Bessel first-order

Fig. 2 presents the variation of the DCS with photon incidence energy for the Bessel second-order and similar nature to Figure 1 but shifting of maxima peak was observed around 3 eV [34] for the $m = 2$ and m=3. On comparing the DCS between harmonic orders, the DCS for the second-order harmonic is consistently lower than that of the first-order harmonic. Also comparing the DCS with Bessel order it is found that Bessel first-order has higher than second order. This is because on compare the amplitude of field Bessel second-order has lower ampltiude than first order and as we known field ampltiude is DCS is directly related.

Fig. 3 illustrates the behavior of the DCS with photon energy of the laser field for the Bessel first-order at $m = 2$ and $m = 2$. The DCS exhibits two major peaks when the photon energy exceeds 0.4 eV, as shown in Figure 3(a). In contrast, for the $m = 3$, three distinct peaks are observed when the photon energy exceeds 0.3 eV, as presented in Figure 3(b). The comparative analysis shows that the DCS corresponding to $m = 2$ is consistently higher than that of $m = 3$. DCS is directly proportional to the amplitude of the laser field, higher harmonic orders lead to lower DCS values. Furthermore, the observed peaks are attributed to superpostion interactions of electrons with the laser field in the vicinity of the

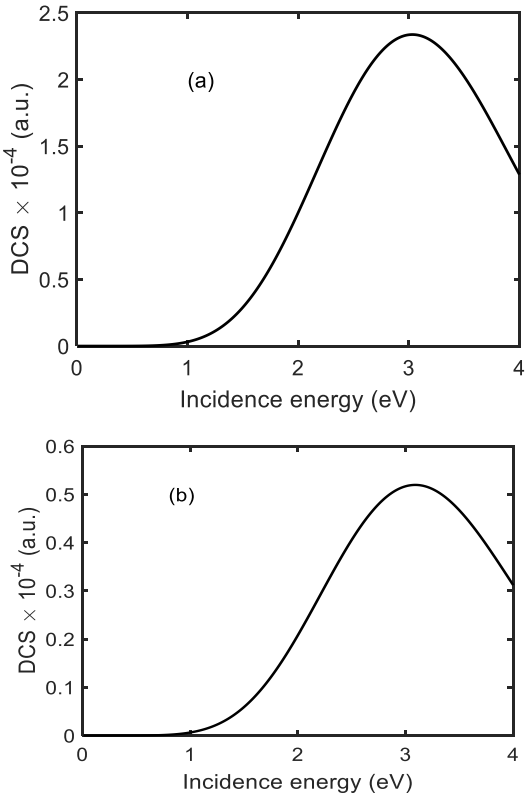

Fig. 2: DCS with incidence energy of electron (a) m=2 and (b) m=3 for Bessel second-order

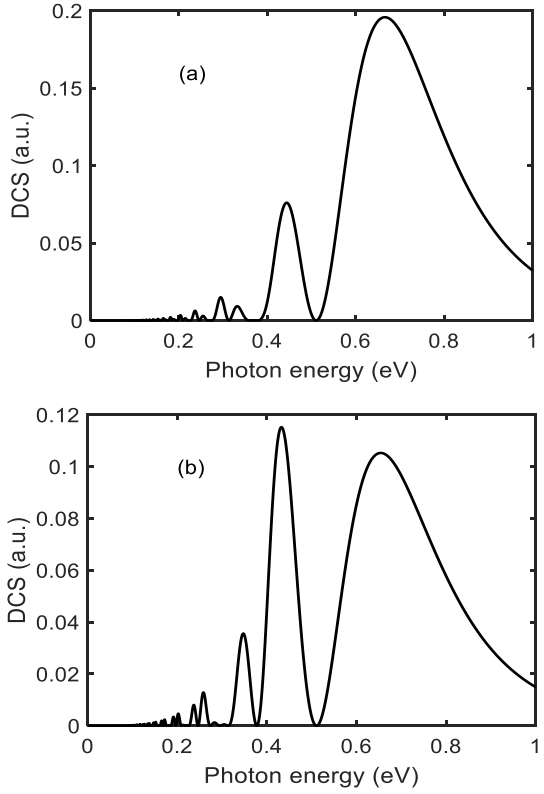

Fig. 3: DCS with photon energy (a) $m = 2$ and (b) $m = 3$ for Bessel first-order

target. The sharp and high peak of DCS is due to field amplitude of scattering particles. The analysis of Figure 3 reveals that the number of peaks in the DCS increases with harmonic order: two major peaks for $m = 2$ and three peaks for $m = 3$. However, the overall amplitude of the DCS decreases with higher harmonic order due to the reduction in field oscillation strength. These findings highlight the intricate role of harmonic order and superposition effects in shaping scattering dynamics under a laser-assisted environment.

Fig. 4 presents the DCS as a function of photon energy for the Bessel second-order. The overall trend is similar to that observed in Fig. 3 with larger number of small peaks the small peaks are the superpostion of smaller amplitude of scattering particle because the particle during scattering looses and gain the energy.
Figus. 4(a) and 4(b) reveal that as the harmonic order increases, smaller peaks become more pronounced. Another key observation is the shift of the peaks towards lower photon energies with increasing harmonic order. For instance, at $m = 3$, a peak appears below 0.4 eV, accompanied by several small-amplitude oscillatory peaks at even lower photon energies.

The combined influence of harmonic order and Bessel order enhances oscillatory structures in the DCS, while simultaneously reducing the overall amplitude due to diminished field strength. The observed peak shifts toward lower photon energies with increasing harmonic order highlight the sensitivity of scattering dynamics to multiphoton resonance processes.

Fig. 5 illustrates the variation of the DCS with scattering angle for the Bessel first-order at different harmonic orders. The results show that the DCS decreases for both the $m = 2$ and $m = 3$, as seen in Figures 5(a) and 5(b), respectively. The DCS for the $m = 2$ is consistently higher than that of $m = 3$, which can be explained by the reduction in field amplitude with increasing harmonic order. Physically, a lower DCS indicates stronger interactions between scattering particles and a reduced probability of scattering, as the interacting particles are closer together. Conversely, a higher DCS corresponds to weaker interactions and a greater probability of scattering, since the particles are relatively farther apart. Das and Dhobi [35] study the differential cross-section of scattering by using Gaussian potential in presence of laser and with linear polarization found decrease with scattering angle. Ghoshal and Ho [36] study positron scattering from hydrogen atomembedded in weakly-coupled plasmas and found the DCS decrease with incresing scattering angle.

This behavior arises because as the Bessel order increases, the amplitude of the field oscillation decreases. Interestingly, after a certain Bessel order, the DCS becomes nearly constant. This suggests that at this regime the interacting particles no longer move closer to each other, as the electrostatic interaction energy between them reaches a value comparable to the rest energy of the particles. This point acts as a reference threshold beyond which the incident particles cannot penetrate or approach the target field any further. In other words, the target field becomes dominant over the incident field, leading to a saturation of the scattering process.

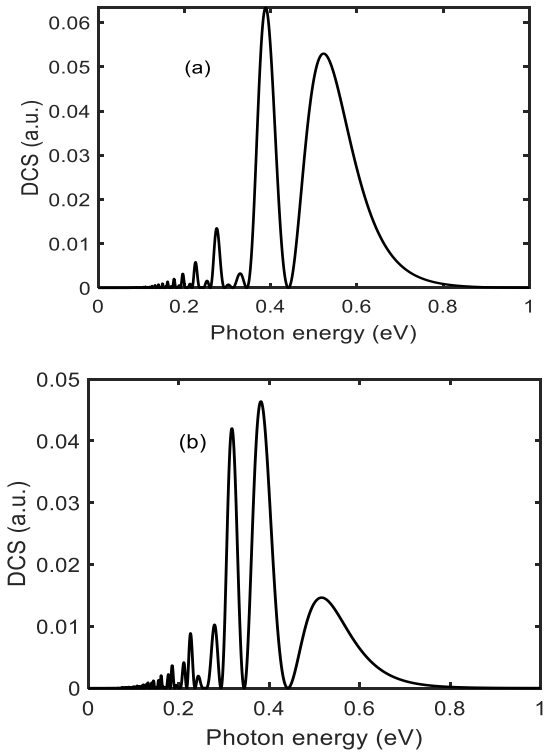

Figure 4: DCS with photon energy (a) $m = 2$ and (b) $m = 3$ for Bessel second-order

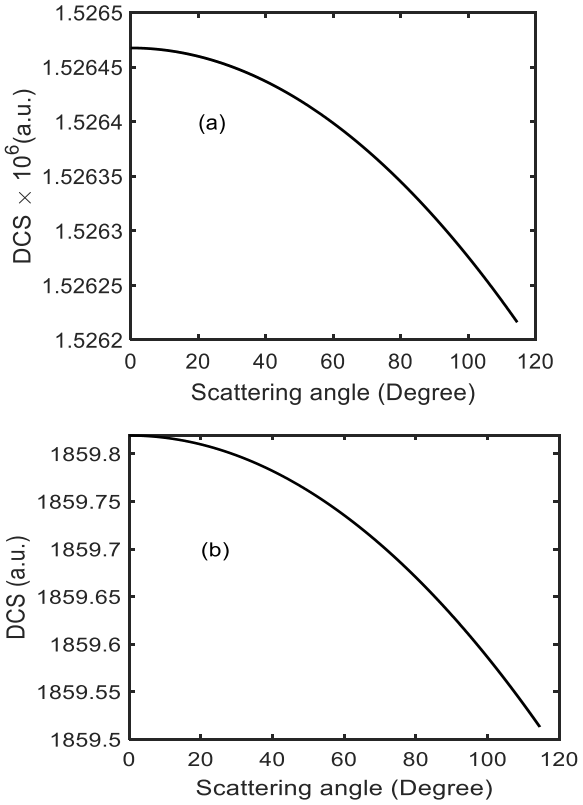

Fig. 5: DCS with scatterionga angle (a) n=1 and (b) n=2 for Bessel order.

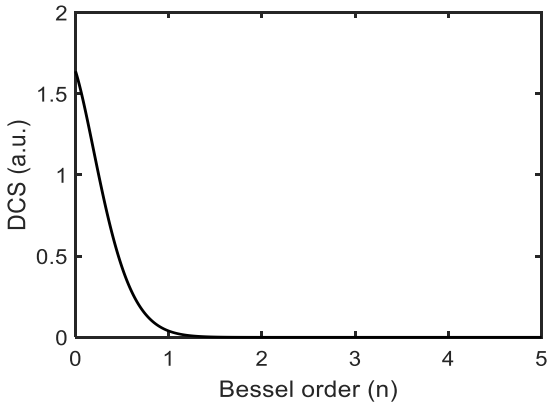

Fig. 6: DCS with different order Bessel order

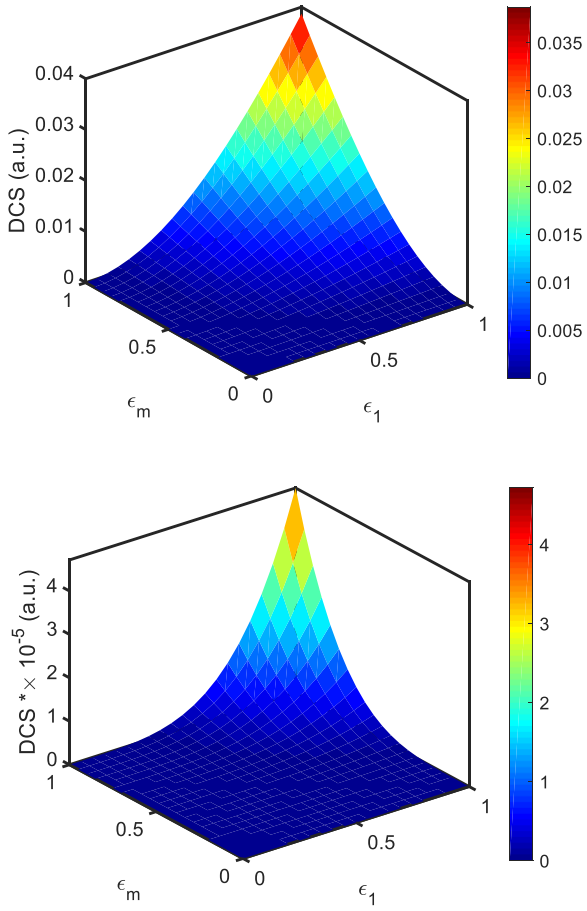

Fig. 7: 3D DCS with polarization vector at n=1 (upper-side) and n=2 (lower side).

Fig. 6 shows the variation of the DCS with increasing order of the Bessel order for both lower and higher harmonic orders. The obseravtion shows the DCS decreases with increasing Bessel order, and the magnitude of the DCS for the lower harmonic order is

consistently higher than that for the higher harmonic order. This behavior arises because as the Bessel order increases, the amplitude of the field oscillation decreases. Interestingly, after a certain Bessel order, the DCS becomes nearly constant. This suggests that at this regime the interacting particles no longer move closer to each other, as the electrostatic interaction energy between them reaches a value comparable to the rest energy of the particles. This point acts as a reference threshold beyond which the incident particles cannot penetrate or approach the target field any further. In other words, the target field becomes dominant over the incident field, leading to a saturation of the scattering process.

Fig. 7 presents the three-dimensional distribution of the DCS as a function of unit vectors for the Bessel first- and second-order. The results show that when the magnitude of the unit vector is lower, the DCS attains higher values, indicating stronger scattering at smaller vector components. A comparison between Bessel order eveals that the DCS for the Bessel first-order is consistently higher than that of the second order. Similarly, when comparing harmonic orders, the DCS corresponding to lower-order harmonics is higher than that of higher-order harmonics. This behavior aligns with the general trend that increasing either the Bessel order or the harmonic order reduces the field amplitude, and consequently decreases the DCS.

4. CONCLUSION

The present analysis reveals that harmonic and Bessel order fundamentally govern the strength and angular characteristics of electron scattering in bichromatic laser fields. The observed correlation between field amplitude reduction and diminishing DCS values highlights the tunability of scattering processes through external laser parameters. This tunability offers potential control mechanisms for designing precise electron–laser interaction systems, relevant to plasma diagnostics, nanostructure fabrication, and high-resolution spectroscopy. Physically, the shift and broadening of resonance peaks with increasing harmonic order indicate altered energy absorption dynamics that can be exploited for studying nonlinear multiphoton processes. Future extensions of this work could incorporate Coulomb potentials to account for long-range interactions, relativistic corrections for high-energy regimes, and comparisons with experimental data to validate the theoretical framework. Such developments would deepen understanding of laser-assisted collision phenomena and support the advancement of next-generation light–matter interaction technologies.

AUTHOR CONTRIBUTIONS

S.K. Das and S.H. Dhobi equally contributed to identifying the research problem, designing the methodology, preparing the original draft, performing computations, and preparing the reviewer report.

FUNDING SOURCES

No fund.

ETHICAL ISSUES

This study did not involve human participants or animal experiments. The research complies with ethical standards for theoretical and computational studies, and all data presented are original.

ACKNOWLEDGMENTS

The authors would like to thank all faculty members of the Department of Physics, Patan Multiple Campus, Tribhuvan University, Patandhoka, Lalitpur, Nepal, for providing a peaceful environment and necessary research facilities during the course of this study.

REFERENCES

[1] N.B. Shrestha, S.P. Gupta, Y. Poudel, K. Yadav, S.H. Dhobi, J.J. Nakarmi, Laser assist scattering in Lennard–Jones potential, *Hadronic Journal*, **46** (4) (2023) 459-462. https://doi.org/10.29083/HJ.46.04.2023/SC459

[2] K.J. LaGattuta, Laser-assisted scattering from a one-dimensional δ-function potential: an exact solution, *Physical Review A*, **49** (3) (1994) 1745. https://doi.org/10.1103/PhysRevA.49.1745

[3] P. Francken, C.J. Joachain, Theoretical study of electron–atom collisions in intense laser fields, *Journal of the Optical Society of America B*, **7**(4) (1990) 554–563. https://doi.org/10.1364/JOSAB.7.000554

[4] B. Wallbank, J.K. Holmes, Laser-assisted elastic electron–atom collisions, *Physical Review A*, **48** (4) (1993) R2515. https://doi.org/10.1103/PhysRevA.48.R2515

[5] K.C. Kulander, J. Cooper, K.J. Schafer, Laser-assisted inelastic rescattering during above-threshold ionization, *Physical Review A*, **51** (1) (1995) 561. https://doi.org/10.1103/PhysRevA.51.561

[6] F. Anis, V. Roudnev, R. Cabrera-Trujillo, B.D. Esry, Laser-assisted charge transfer in He^{2+} + H collisions, *Physical Review A*, **73** (4) (2006) 043414. https://doi.org/10.1103/PhysRevA.73.043414

[7] D.B. Milošević, D. Bauer, W. Becker, Quantum-orbit theory of high-order atomic processes in intense laser fields, *Journal of Modern Optics*, **53** (1–2) (2006) 125–134. https://doi.org/10.1080/09500340500186099

[8] R. Daniele, G. Ferrante, Particle scattering in the presence of a strong multimode laser field, *Journal of Physics B: Atomic and Molecular Physics*, **14** (20) (1981) L635. DOI 10.1088/0022-3700/14/20/004

[9] G.L. Yudin, M.Y. Ivanov, Physics of correlated double ionization of atoms in intense laser fields: quasistatic tunneling limit, *Physical Review A*, **63** (3) (2001) 033404. https://doi.org/10.1103/PhysRevA.63.033404

[10] P.H. Bucksbaum, M. Bashkansky, T.J. McIlrath, Scattering of electrons by intense coherent light, *Physical Review Letters,* **58** (4) (1987) 349. https://doi.org/10.1103/PhysRevLett.58.349

[11] S.M. Metev, V.P. Veiko, *Laser-Assisted Microtechnology*, **19**, Springer Sci. & Bus. Media, 2013.

[12] S. Varró, F. Ehlotzky, Potential scattering of electrons in a bichromatic laser field of frequencies ω and 2ω or ω and

3ω, *Optics Communications*, **99** (3–4) (1993) 177–184. https://doi.org/10.1016/0030-4018(93)90075-G.

[13] A. Cionga, F. Ehlotzky, M. Florescu, M. Iacomi, One-dimensional potential scattering of electrons in a bichromatic laser field, *Journal of Physics B: Atomic, Molecular and Optical Physics*, **34** (20) (2001) 3951–3962. https://doi.org/10.1088/0953-4075/34/20/307.

[14] D.B. Milošević, Potential scattering in a strong multicolour laser field, *Journal of Physics B: Atomic, Molecular and Optical Physics*, **29** (4) (1996) 875–893. https://doi.org/10.1088/0953-4075/29/4/024.

[15] R.P. Kurmi, K. Yadav, A. Shrestha, S.H. Dhobi, Laser assist quantum dot scattering with Gaussian potential, *Physics Open*, **23** (2025) 100267. https://doi.org/10.1016/j.physo.2025.100267.

[16] S.T. Zhang, J. Chen, L. Shu-min, The intensity dependence of the free-free transition in a bichromatic laser field, *Canadian Journal of Physics,* **80** (9) (2002) 969–977. https://doi.org/10.1139/p02-052.

[17] S. Kerbstadt, K. Eickhoff, T. Bayer, M. Wollenhaupt, Bichromatic control of free electron wave packets, *In Progress in Ultrafast Intense Laser Science XV, Cham: Springer International Publishing* (2020) 43–76. https://doi.org/10.1007/978-3-030-47098-2_3.

[18] B. Zhou, M.-Y. Zheng, D.-Y. Wen, The second Born approximation of electron–argon elastic scattering in a bichromatic laser field, *arXiv* (2013). https://doi.org/10.48550/arXiv.1301.4661.

[19] Z. Zun-Lue, L. Ming-Chao, S. Jin-Feng, Electron–helium atom collisions in the presence of a bichromatic laser field, *Communications in Theoretical Physics,* **50** (2) (2008) 477–480. https://doi.org/10.1088/0253-6102/50/2/39.

[20] P. Liu, Q. Wang, X. Li, Studies on CdSe/L-cysteine quantum dots synthesized in aqueous solution for biological labeling, *The Journal of Physical Chemistry C*, **113** (18) (2009) 7670–7676. https://doi.org/10.1021/jp901292q.

[21] J. Maurer, U. Keller, Ionization in intense laser fields beyond the electric dipole approximation: concepts, methods, achievements and future directions, *Journal of Physics B: Atomic, Molecular and Optical Physics*, **54** (9) (2021). DOI 10.1088/1361-6455/abf731

[22] S.H. Dhobi, S.P. Gupta, K. Yadav, A.K. Jha, Scattering dynamics in thermal environments around PEMFC electrode, *International Energy Journal,* **25** (1A) (2025) 123-132. http://rericjournal.ait.ac.th/index.php/reric/article/view/3082/pdf

[23] S.H. Dhobi, K. Yadav, S.P. Gupta, J.J. Nakarmi, A.K. Jha, Non-monochromatic laser assist scattering in thermal environment, *Journal of the Nigerian Society of Physical Sciences,* **7** (1) (2025) 2345–2345. https://doi.org/10.46481/jnsps.2025.2345

[24] S.H. Dhobi, S.P. Gupta, K. Yadav, J.J. Nakarmi, A.K. Jha, Differential cross section with Volkov–thermal wave function in Coulomb potential, *Atom Indonesia*, **50** (1) (2024) 19–25. https://doi.org/10.55981/aij.2024.1309

[25] I.F. Barna, S. Varró, Laser-assisted proton collision on light nuclei at moderate energies, *Laser and Particle Beams,* **33** (2) (2015) 299–305. https://doi.org/10.1017/S0263034615000191

[26] N.M. Kroll, K.M. Watson, Charged-particle scattering in the presence of a strong electromagnetic wave, *Physical Review A*, **8** (1973) 804–809. https://doi.org/10.1103/PhysRevA.8.804

[27] S.H. Dhobi, S.P. Gupta, J.J. Nakarmi, B. Koirala, K. Yadav, S.K. Oli, M. Gurung, Scattering of free electrons with hydrogen atoms in proton exchange membrane fuel cell system, *International Annals of Science*, **13** (1) (2023) 22–28. https://doi.org/10.21467/ias.13.1.22-28

[28] S.H. Dhobi, J.J. Nakarmi, K. Yadav, S.P. Gupta, B. Koirala, A.K. Shah, Study of thermodynamics of a thermal electron in scattering, *Heliyon*, **8** (12) (2022). https://doi.org/10.1016/j.heliyon.2022.e12315

[29] B.K. Agrwal, H. Prakash, *Quantum Mechanics*, Prentice Hall of India Pvt. Ltd., New Delhi (2002).

[30] K. Kavazović, A. Čerkić, D.B. Milošević, Electron–molecule scattering in a bichromatic elliptically polarised laser field: plateau structures and two-centre interference minima, *Molecular Physics*, **119** (14) (2021) e1948123. https://doi.org/10.1080/00268976.2021.1948123

[31] S.H. Dhobi, K. Yadav, S.P. Gupta, J.J. Nakarmi, B. Koirala, Differential cross-section in the presence of a weak laser field for inelastic scattering, *Ukrainian Journal of Physics,* **67** (4) (2022) 227–227. https://doi.org/10.15407/ujpe67.4.227

[32] S.H. Dhobi, K. Yadav, A.K. Jha, B. Karki, J.J. Nakarmi, Free electron–ion interaction and its effect on output current of permeable exchange membrane hydrogen fuel, *ECS Trans.*, **107**(1) (2022) 8457. https://doi.org/10.1149/10701.8457ecst

[33] D. Habibović, A. Čerkić, D.B. Milošević, Laser-assisted electron–atom scattering in an orthogonally polarized two-color laser field, *The European Physical Journal D*, **79**(11) (2025) 136. https://doi.org/10.1140/epjd/s10053-025-01087-7

[34] K. Bartschat, J. Tennyson, O. Zatsarinny, Quantum-mechanical calculations of cross sections for electron collisions with atoms and molecules, *Plasma Processes and Polymers*, **14**(1–2) (2017) 1600093. https://doi.org/10.1002/ppap.201600093

[35] S.K. Das, S.H. Dhobi, Study of the differential cross-section of scattering by using Gaussian potential in presence of laser, *Patan Prospective Journal*, **5** (1) (2025) 120–132. https://doi.org/10.3126/ppj.v5i1.85843

[36] A. Ghoshal, Y.K. Ho, Positron scattering from hydrogen atom embedded in weakly-coupled plasmas, *The European Physical Journal D*, **55** (3) (2009) 581–589. https://doi.org/10.1140/epjd/e2009-00238-x